Forest Height Feature Extraction in Polarimetric SAR Interferometry by using Rotational Invariance Property

Hiroyoshi Yamada, Yoshio Yamaguchi
Faculty of Engineering, Niigata University
line 2: name of organization, acronyms acceptable
Niigata, 950-2181 Japan
{yamada,yamaguch}@ie.niigata-u.ac.jp

Wolfgang Martin Boerner
The University of Illinois at Chicago
UIC-ECE/CSN
Chicago, IL 60607-718 USA
boerner@ece.uic.edu

Abstract— **This paper present a new forest height feature extraction technique for single baseline polarimetric and interferometric SAR data. The authors have proposed polarimetric SAR interferometry based on the ESPRIT algorithm. However, the algorithm assumes that there exist dominant polarized components in both the ground and canopy. Hence, estimated interferometric phase of local scattering centers may be slightly biased when forest components are highly depolarized. In this report, we examine effect of depolarized components of forest in ESPRIT-based polarimetric SAR interferometry. Numerical examples show that the effective scenario for the algorithm. Also, we present an alternative derivation of the ESPRIT-type algorithm which helps us understand how the ESPRIT algorithm works for depolarized components. Experimental results by using E-SAR data are also provided to show the performance of the ESPRIT estimation.**

Keywords-polarimetric SAR interferometry; forest canopy; ESPRIT algorithm; polarized and depolarized components

I. INTRODUCTION

Synthetic aperture radar (SAR) interferometry has been widely used to obtain digital elevation maps (DEM) over terrain [1]. The SAR interferometry is sensitive primarily to the vertical structure of vegetated land surface [2]. On the other hand, radar polarimetry is sensitive essentially to the shape, orientation and dielectric constant of vegetation scatterer. Cloude and Papathanassiou have proposed the polarimetric SAR interferometry for forest biomass estimation (tree height and canopy extinction coefficent, *etc.*) which is more sensitive to distribution of the oriented scatterers than either radar polarimetry or interferometry alone [3][4].

We have proposed the ESPRIT-based polarimetric SAR interferometry [5]-[7]. The ESPRIT algorithm is one of the superresolution techniques, and is widely used for direction of arrival estimation with an antenna array [8]. When we apply the algorithm to polarimetric and interferometric data of forest area, interferometric phases corresponding to the ground and the canopy can be obtained directly without solving nonlinear equations [4]. Experimental results by NASA-JPL SIR-C/X-SAR data and DLR E-SAR data have reported in [5]-[7]. These results show that the algorithm works fine with adequate number of multilooks for actual SAR data. However, when we check the results precisely, tree height was estimated slightly low (*i.e.* phase difference becomes small) than the real height in some areas. Such areas are increased when the number of multilooks exceeds an adequate number. Change of the incident angle and noise may cause such a bias, however, there seems to be the other dominant causes. That must be depolarized scattering components from the canopy.

In this paper, we derive an another derivation of the ESPRIT-based polarimetric SAR interferometry and show that how the depolarized component affects in the interferometric phase estimation. We derive theoretically that the ESPRIT estimation is biased for the data including depolarized components. However, we show by some numerical results that the bias due to depolarized components is sufficiently small when the depolarized component is smaller than the polarized components. At the L-band observations for forest, polarized ground components strong. This is why the ESPRIT algorithm is applicable to the L-band data.

II. DATA MODEL

In interferometric observations, the observed backscattered data can be modeled by the sum of dominant local scattered waves from the ground and the canopy. Here we formulate the model for completely polarized waves and depolarized waves. Noise components are ignored for simplicity. Another models can be easily derived by using the following models.

A. Complately polarized waves

When both the ground and canopy are completely polarized and have local interferometric phase ϕ_1 and ϕ_2, respectively, the observed data in HH, HV, and VV channels at antenna 1 and 2 can be written by

$$\begin{aligned} \boldsymbol{E}_1 &= [E_{hh1}, E_{hv1}, E_{vv1}]^T = \boldsymbol{S} \\ \boldsymbol{E}_2 &= [E_{hh2}, E_{hv2}, E_{vv2}]^T = \boldsymbol{SD} \end{aligned} \tag{1}$$

where $\boldsymbol{S}=[\boldsymbol{s}_1, \boldsymbol{s}_2]$ is a 3x2 polarization state matrix whose columns contain normalized polarization state vector of the ground ($\boldsymbol{s}_1$) and the canopy ($\boldsymbol{s}_2$), and $\boldsymbol{D}=diag\{e^{j\phi}{}_1, e^{j\phi}{}_2\}$ is an interferometric phase matrix. T denotes transpose.

The overall data vector and its correlation matrix can be defined by

$$\boldsymbol{x} = \begin{bmatrix} \boldsymbol{E}_1 \\ \boldsymbol{E}_2 \end{bmatrix} = \begin{bmatrix} \boldsymbol{S} \\ \boldsymbol{SD} \end{bmatrix}, \tag{2}$$

$$\boldsymbol{R}_{pol} = \left\langle \boldsymbol{x}\boldsymbol{x}^H \right\rangle = \begin{bmatrix} \boldsymbol{SIS}^H & \boldsymbol{SID}^H\boldsymbol{S}^H \\ \boldsymbol{SDIS}^H & \boldsymbol{SIS}^H \end{bmatrix} = \begin{bmatrix} \boldsymbol{R}_{11} & \boldsymbol{R}_{21}^H \\ \boldsymbol{R}_{21} & \boldsymbol{R}_{11} \end{bmatrix}, \tag{3}$$

where H denotes complex conjugation and $\boldsymbol{I}$ is an identity matrix.

B. Depolarized waves

Since no dominant polarized components cannot be observed in the depolarized waves, the correlation matrix of a scattered wave can be modeled by

$$\boldsymbol{R}_{depol} = \begin{bmatrix} \boldsymbol{R}_{11} & \boldsymbol{R}_{21}^H \\ \boldsymbol{R}_{21} & \boldsymbol{R}_{11} \end{bmatrix} = \begin{bmatrix} \boldsymbol{R}_{11}^{depol} & \boldsymbol{R}_{11}^{depol} e^{j\phi_d} \\ \boldsymbol{R}_{11}^{depol} e^{-j\phi_d} & \boldsymbol{R}_{11}^{depol} \end{bmatrix}. \tag{4}$$

In this case, the $\boldsymbol{R}_{11}$ becomes a diagonal matrix of full rank. This is a model for one depolarized wave having interferometric phase of ϕ_d. When there exist two or more depolarized local scatterers, the overall correlation matrix can be modeled by the sum of their correlation matrix.

III. ESPRIT ALGORITHM FOR POLARIZED AND DEPOLARIZED WAVES

In the formulation of the polarimetric SAR interferometry based on the TLS-ESPRIT algorithm, we only considered polarized components [6]. To include the depolarized waves in the formulation, it is better to use conventional ESPRIT expressions [10]. In the conventional ESPRIT algorithm, we first define a 3x3 matrix $\boldsymbol{C}$ as

$$\boldsymbol{C} = \boldsymbol{R}_{11} - \gamma \boldsymbol{R}_{21} \tag{5}$$

where $\gamma = e^{j\phi}$. From (3) and (4), it is easy to derive that a local component can be removed in $\boldsymbol{C}$ when γ coincides with its interferometric phase. In such a case rank of $\boldsymbol{C}$ decreases when the matrix contains only polarized components or one depolarized only. To check the rank condition of $\boldsymbol{C}$, we define following scanning function.

$$P_{ESPRIT}(\phi) = 1 / \prod_{i=1}^{d} \lambda_i(\phi) \tag{6}$$

where $\lambda_1(\phi) > .. > \lambda_d(\phi)$ are the eigenvalues of $\boldsymbol{C}$ at ϕ, and d is rank of $\boldsymbol{R}_{11}$ that can be easily estimated by the number of dominant eigenvalues of the overall correlation matrix. Denominator of this function becomes zero at each interferometric phase. Interferometric phases can be estimated by the peaks of the function.

For the data having both several polarized components and one depolarized component, (5) becomes

$$\boldsymbol{C} = \boldsymbol{A}(\boldsymbol{I} - \gamma \boldsymbol{D}^H)\boldsymbol{A}^H + (1 - \gamma e^{-j\phi_d})\boldsymbol{R}_{11}^{depol}. \tag{7}$$

In this case, (6) cannot becomes infinite when ϕ coincides with the interferometric phase of polarized components because the full rank matrix $\boldsymbol{R}_{11}^{depol}$ component still remains. Therefore the peak becomes dull and is often biased to the phase of depolarized components. On the other hand, when ϕ coincides with the interferometric phase of depolarized components, the rank of C becomes number of the polarized components. Typically number of polarized components may be 1 or 2 located at the ground and/or canopy, therefore phase corresponding to the canopy will be correctly estimated when we use 3 components of an overall data correlation matrix.

IV. NUMERICAL AND EXPERIMENTAL RESULTS

To examine effect of depolarized components for interferometric phase extraction by the ESPRIT algorithm, we show two numerical examples. In the first examples, *model I*, we assume that there exist a completely polarized (ground) components located at ϕ_1 = 90 degree and a depolarized (canopy) components at ϕ_d = 150 degree. For simplicity we also assume diagonal elements of $\boldsymbol{R}_{11}^{depol}$ are the same. Figure 1 shows the estimation results of (6) with d = 3 for several power combinations of the polarized and depolarized components. The value m in Fig.1 denotes the effective ground-to-volume amplitude ratio (m= total power from the ground/ total power from the canopy). As discussed in the previous section, a strong peak appears at the interferometric phase corresponding to the depolarized component. The peaks of the polarized component become small and large phase bias occur in large m. From this model we can say that the phase bias is negligibly small when m > 3dB. In the second example, *model II*, one completely polarized component at 90 degree and one partially polarized component at 150 degree at are employed. The partially component are modeled as the sum of polarized and depolarized components of the same total power contribution having the same interferometric phases. Estimated

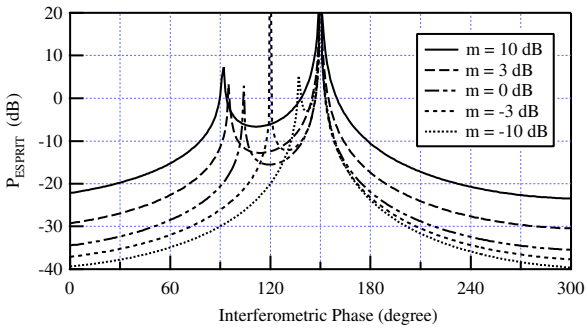

Figure 1. Interferometric phase estimation by using (6) (*model I*)

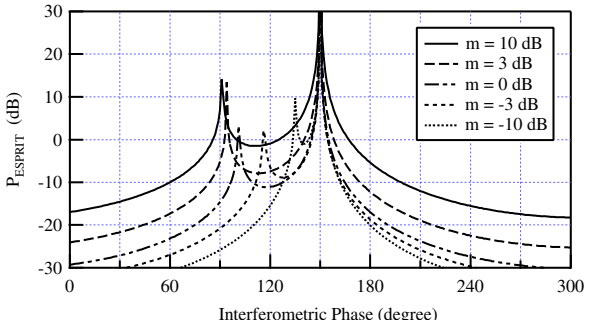

Figure 2. Interferometric phase estimation by using (6) (*model II*)

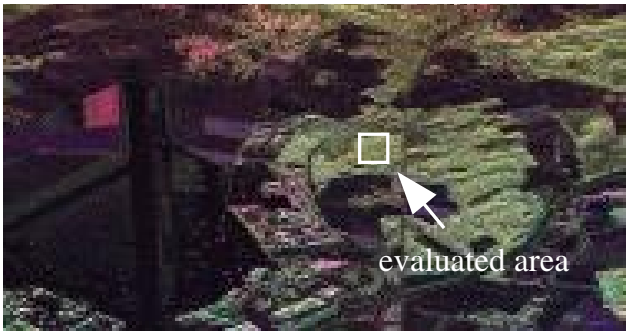

Figure 3. The test-site image of E-SAR L-band data

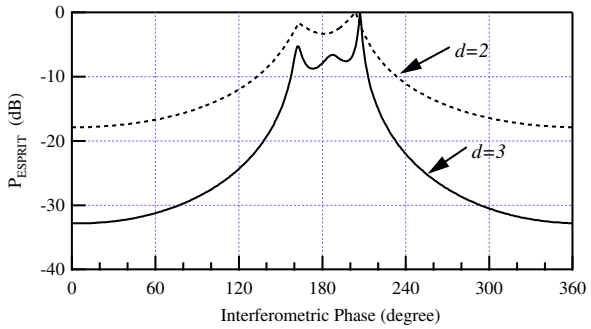

Figure 4. Interferometric phase estimation by using (6) of the evaluated area.

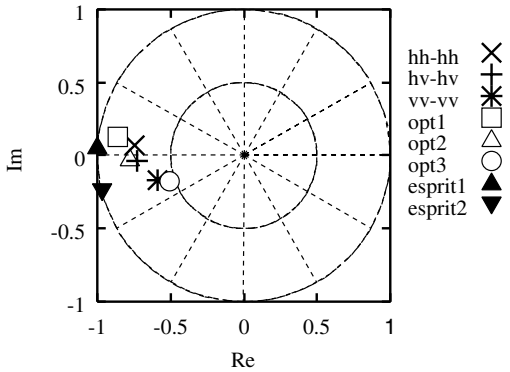

Figure 5. Interferometric phases estimated by TLS-ESPRIT and conventional polarimetric SAR interferometry.

bias is also negligibly small when m > 3dB in this model. Several different models were also tested. The ESPRIT algorithm works properly when m > 3 dB in almost all models having two local scattering centers. Total power image of an experimental data at oberfaffenhofen test-site by the E-SAR (DLR) is shown in Fig.3. Figure 4 shows a typical estimation results by using (6) . The picked up area was denoted in Fig.3. The TLS-ESPRIT results for $d = 2$ are shown in Fig.5, where interferometric phases of each channel and their optimum phases [3] are also shown. The estimated phases of TLS-ESPRIT algorithm are biased. P_{ESPRIT} in Fig.4 also becomes dull and biased, which may be caused by depolarized component(s). The bias is decrease and fine peaks appear when we apply the ESPRIT with $d = 3$.

V. CONCLUSIONS

An alternative derivation of the ESPRIT-type algorithm for polarimetric SAR interferometry is introduced to analyze phase bias due to depolarized components. This helps us how the ESPRIT algorithm works with mixture of polarized and depolarized wave scatterings from forest canopies. When there exist both polarized and depolarized components, bias will be caused. However, numerical results show that the phase bias is permissively small when the effective ground-to-volume amplitude ratio is higher than 3 dB. The ground components will be dominant at the L-band observations, therefore, the ESPRIT algorithm works properly in almost all forested area.

REFERENCES

[1] P.A.Rosen, S.Hensley, I.R.Joughin, F.K.Li, S.N.Madsen, E.Rodriguez, and R.M.Goldstein, "Synthetic Aperture Radar Interferometry," Proc. IEEE, vol. 88, no.3, pp. 333–382, March 2000.

[2] R.N.Treuhaft, S.N.Madsen, M.Moghaddam, and J.J.van Zyl, "Vegetation characteristics and surface topography from interferometric radar," Radio Sci., vol.31, pp.1449-1485, Nov./Dec. 1996.

[3] S.R.Cloude and K.P.Papathanassiou, "Polarimetric SAR interferometry," IEEE Trans. Geosci. Remote Sens., vol.36, no.5, pp. 1551-1565, Sept. 1998.

[4] K.P.Papathanassiou and S.R.Cloude, "Single-baseline polarimetric SAR interferometry," IEEE Trans. Geosci. Remote Sens., vol.39, no.11, pp. 2352-2363, Nov. 2001.

[5] H.Yamada, Y.Yamaguchi, E.Rodriguez, Y.Kim and W.M.Boerner, "Polarimetric SAR interferometry for forest canopy analysis by using the super-resolution methoid," Proc. IGARSS 2001, on CD-ROM, July 2001.

[6] H.Yamada, Y.Yamaguchi, E.Rodriguez, Y.Kim and W.M.Boerner, "Polarimetric SAR interferometry for forest analysis based on the ESPRIT algorithm," IEICE Trans. Electron., vol.E-84-C, no.12, pp. 1917-1924, Dec.2001

[7] K.Sato, H.Yamada, and Y.Yamaguchi, "Advantage of the ESPRIT method in polarimetric interferometry for forest analysis," IEICE Trans. Commun., vol.E86-B, no.5, pp.1666-1672, May 2003.

[8] R.Roy and T.Kailath, "ESPRIT -- Estimation of signal parameters via rotational invariance technique," IEEE Trans. Acoust., Speech Signal Process., vol.37, no.7, pp.984-995, July 1989.

[9] D.Kasilingam, M.Nomula, and S.Cloude, "A technique for removing vegetation bias from polarimetric SAR Interferometry," Proc. IGARSS 2002, on CD-ROM, July 2002.

[10] R.Roy, A.Paulraj, and T.Kailath, "ESPRIT -- A subspace rotation approach to estimation of parameters of cisoids in noise," IEEE Trans. Acoust., Speech Signal Process., vol.ASSP-34, no.5, pp.1340-1342, Oct. 1986.